Article

Current Biology

Encoding of Multiple Reward-Related Computations in Transient and Sustained High-Frequency Activity in Human OFC

Highlights

- High-frequency activity in human OFC reflects multiple valuation computations
- Transient or sustained encoding modes support present or past reward information
- Encoding occurred in central and lateral OFC without fine anatomical organization
- Results support representation of a complex task state in human OFC

Authors

Ignacio Saez, Jack Lin, Arjen Stolk, ..., Gerwin Schalk, Robert T. Knight, Ming Hsu

Correspondence

rtknight@berkeley.edu (R.T.K.), mhsu@haas.berkeley.edu (M.H.)

In Brief

Saez et al. carried out intracranial recordings in the OFC of human patients while they played a decision-making task and demonstrate that high-frequency activity in OFC reflects a variety of task-related computations, supporting the idea of a task state representation.

Saez et al., 2018, Current Biology *28*, 1–11
September 24, 2018
https://doi.org/10.1016/j.cub.2018.07.045

CellPress

Please cite this article in press as: Saez et al., Encoding of Multiple Reward-Related Computations in Transient and Sustained High-Frequency Activity in Human OFC, Current Biology (2018), https://doi.org/10.1016/j.cub.2018.07.045

Current Biology
Article

Encoding of Multiple Reward-Related Computations in Transient and Sustained High-Frequency Activity in Human OFC

Ignacio Saez,[1] Jack Lin,[2] Arjen Stolk,[1] Edward Chang,[3] Josef Parvizi,[4] Gerwin Schalk,[5] Robert T. Knight,[1,*] and Ming Hsu[1,6,*]
[1]University of California, Berkeley, Berkeley, CA 94720, USA
[2]University of California, Irvine, Irvine, CA 92697, USA
[3]University of California, San Francisco, San Francisco, CA 94143, USA
[4]Stanford University, Stanford, CA 94305, USA
[5]Wadsworth Center, New York State Department of Health, Albany, NY 12201, USA
[6]Lead Contact
*Correspondence: rtknight@berkeley.edu (R.T.K.), mhsu@haas.berkeley.edu (M.H.)
https://doi.org/10.1016/j.cub.2018.07.045

SUMMARY

Human orbitofrontal cortex (OFC) has long been implicated in value-based decision making. In recent years, convergent evidence from human and model organisms has further elucidated its role in representing reward-related computations underlying decision making. However, a detailed description of these processes remains elusive due in part to (1) limitations in our ability to observe human OFC neural dynamics at the timescale of decision processes and (2) methodological and interspecies differences that make it challenging to connect human and animal findings or to resolve discrepancies when they arise. Here, we sought to address these challenges by conducting multi-electrode electrocorticography (ECoG) recordings in neurosurgical patients during economic decision making to elucidate the electrophysiological signature, sub-second temporal profile, and anatomical distribution of reward-related computations within human OFC. We found that high-frequency activity (HFA) (70–200 Hz) reflected multiple valuation components grouped in two classes of valuation signals that were dissociable in temporal profile and information content: (1) fast, transient responses reflecting signals associated with choice and outcome processing, including anticipated risk and outcome regret, and (2) sustained responses explicitly encoding what happened in the immediately preceding trial. Anatomically, these responses were widely distributed in partially overlapping networks, including regions in the central OFC (Brodmann areas 11 and 13), which have been consistently implicated in reward processing in animal single-unit studies. Together, these results integrate insights drawn from human and animal studies and provide evidence for a role of human OFC in representing multiple reward computations.

INTRODUCTION

Making decisions under incomplete information is a notoriously difficult problem [1, 2] that relies on representation of multiple types of reward-related computations across prefrontal cortical areas [3–5]. Among these areas, neural activity in human orbitofrontal cortex (OFC) has been consistently shown to represent multiple reward-related computations [6–10]. In particular, neuroimaging studies over the past decade have expanded our knowledge of OFC contributions to decision making, providing a rich characterization of OFC signals consistent with predictions from influential theories on valuation and learning, including those associated with choice value, uncertainty, and counterfactual representations, such as regret [5, 10–12].

Despite this progress, a detailed account of human OFC processes in the human OFC remains elusive, due in part to limitations in our ability to observe neural dynamics at the timescale of decision processes, as well as methodological and interspecies differences that make it challenging to connect human and animal findings or to resolve discrepancies when they arise. First, recent data from model organisms have begun to delineate a more complex picture whereby OFC encodes a much broader variety of information than would be predicted by pure valuation and associative learning accounts. In particular, whereas there is evidence for the existence of valuation and learning signals that reflect integration of all relevant decision features, such as probability, reward magnitude, prior expectations, etc., OFC also responds to these value-relevant features in an independent manner that does not reflect overall value or level of reinforcement, which is notably different from the ventral striatum, where integrated representations are prevalent [8, 9]. Indeed, OFC encoding extends even to information such as specific identity of sensory stimuli, which, by themselves, do not carry reinforcing value. However, due to the inherent spatiotemporal limitations of non-invasive techniques, such as fMRI and electroencephalography (EEG), the nature of encoding in the human OFC remains to be defined.

Second, although there is a broad correspondence between human and animal findings on OFC functioning, important discrepancies exist, in particular at the more detailed anatomical level

[9, 13, 14]. Whereas human neuroimaging studies have repeatedly implicated some portions of the OFC, such as ventromedial prefrontal cortex (vmPFC) (Brodmann area 14) during decision making [5, 15], the implication of other regions, including the directly adjacent central OFC (Brodmann regions 11 and 13), has received much less support. In contrast, nonhuman primate studies have found substantial reward-related responses in homologs of central OFC but interestingly little evidence for such encoding in the homologs of the vmPFC [9, 13, 14].

Two sets of hypotheses have been offered for these differences. First, they may arise due to differences in human and animal study procedures, such as the extensive overtraining typical in animal studies, or the common use of secondary reinforcers in human studies, both of which may result in the engagement of different sets of cognitive processes [16]. The second, and non-mutually exclusive, set of possibilities is related to well-known limitations of fMRI measures. Human OFC is known to be particularly vulnerable to motion and sinus air artifacts that can corrupt fMRI signals [17, 18]. In addition, as the blood-oxygen-level-dependent (BOLD) signal is sensitive to both input and output events, vmPFC findings in fMRI may in fact reflect processing elsewhere in upstream regions. Importantly, these issues have different implications for our understanding of human OFC functioning but to date have been difficult to resolve.

Here, we sought to address these challenges by combining the rare opportunity to conduct intracranial recording in neurosurgical patients with the administration of a neuroeconomic task. Specifically, we conducted electrocorticographic (ECoG) recordings of field potentials (FPs) from OFC using multi-electrode strips and grids. ECoG signals capture the activity of hundreds of thousands of neurons at a millisecond temporal resolution and spatial resolution of <1 cm [19]. This intermediate spatiotemporal coverage has been referred to as a "mesoscale" level of analysis, lying between the extensive anatomical coverage of fMRI and the exquisite temporal resolution of single-unit recordings [20–22]. In addition, because electrodes are placed directly on the cortical surface, the resulting signals are not affected by susceptibility artifacts arising near air-tissue boundaries to which OFC is sensitive [17, 18].

In particular, we concentrated on examination of high-frequency activity (HFA) (70–200 Hz) within the broadband FP signal to characterize the nature and anatomical distribution of information encoding across the human OFC. Unlike lower frequency bands that reflect activity in broadly distributed networks [23], growing evidence suggests HFA, which is not observable in traditional scalp EEG due to conduction filtering and source spread, reflects local non-rhythmic synaptic activity [19] and is a key marker of cortical activation [24, 25]. HFA analyses have significantly advanced our understanding of cortical dynamics in a number of domains, including attention, language, memory, and motor control [20–22, 26], but to date, no study to our knowledge has examined the relationship between HFA and decision-making computations in humans [27, 28].

RESULTS

Economic Choice Behavior in Neurosurgical Patients

To probe decision-making processes in our subjects, we combined ECoG recordings in 10 patients with administration of a neuroeconomic task that captures the tradeoff between risk and reward [4, 29]. All patients had medically refractory epilepsy and were implanted with chronic subdural grid and/or strip electrodes as part of a pre-operative procedure to localize the epileptogenic focus, which in none of the patients was judged to be located in OFC (see STAR Methods). As electrode placement and treatment were based solely on the clinical needs of each patient, the specific number and location of electrodes varied across individuals. We recorded from a total of 210 electrodes, of which 192 were included in the final dataset (for details regarding electrode implantation, localization, ECoG recording, and electrophysiological quality control, see STAR Methods; coverage in Figure 1A and individual subject coverage in Figure S1).

Testing was conducted over a single session of 15–20 min in the epilepsy monitoring unit, while paying careful attention to the patient's neurological condition and testing only when the patient was fully alert and cooperative. On each trial, participants were presented with a choice between a sure prize and a risky gamble with a varying probability of higher winnings (Figure 1B; STAR Methods). Although simple, the explicit presentation of risk and reward information across trials allowed us to exert strong experimental control over each decision while minimizing working memory load. Similar tasks have been used in a number of previous neuroimaging studies in healthy human participants to characterize decision-making processes in frontostriatal circuits [4, 29], providing the ability to compare findings across recording methodologies.

For subsequent analyses, we defined two sets of reward-related signals associated with both choice and outcome evaluation processes, respectively, which have been implicated in previous studies (see STAR Methods and Table S1). Choice-related regressors reflected information available during deliberation, namely, (1) the probability of the gamble resulting in a win (win probability); (2) the risk, or variance, associated with the gamble regardless of choice (risk); (3) the expected value of the chosen option (chosen value); and (4) whether the subject chose to gamble (gamble). Outcome evaluation regressors were defined as (1) whether the gamble resulted in a win (win) (2) or a loss (loss), (3) reward prediction error (RPE) (difference between the obtained reward and the expected value of the gamble), and (4) the amount of extra money that would have been won for the non-chosen option (regret).

Behaviorally, we found that subjects were approximately risk neutral, choosing to gamble only slightly more often than a risk neutral baseline model (55.9% ± 8.5% of risky choices). The proportion of risky choices increased as the offer value (win probability) increased, which was well captured by a logit model of decision under risk ($p < 0.001$; random effects logit analysis; Figure 1C). Importantly, a comparison of behavior from patients undergoing intracranial recording with those from 10 healthy comparison participants (see STAR Methods) shows that patterns of behavior were comparable at both level of sensitivity of risk-reward tradeoff (Figures 1C and S1) and reaction time (Figure S2).

OFC HFA Reflects Choice- and Outcome-Related Valuation Signals

Next, we sought to connect neural responses in OFC to valuation components related to choice and outcome processing.

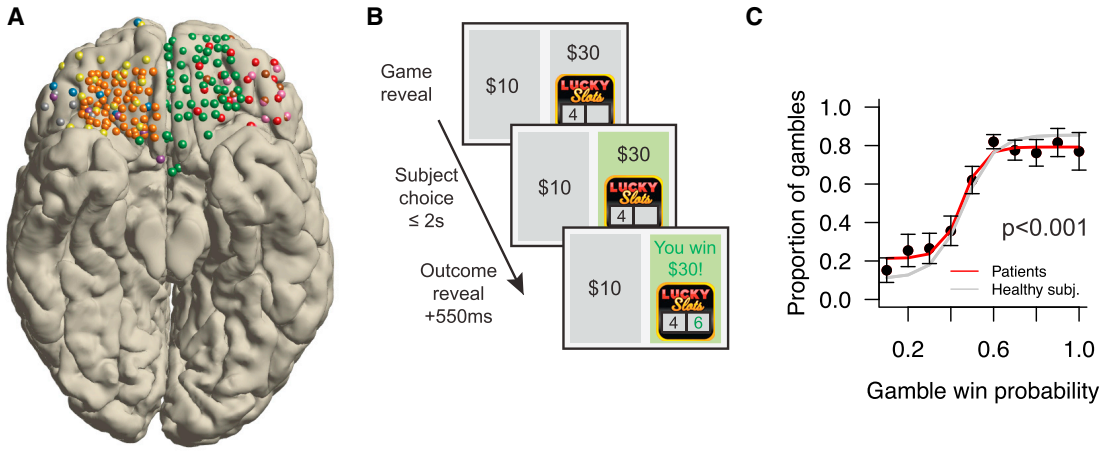

Figure 1. Experimental Approach

(A) Anatomical reconstruction showing placement of all 192 ECoG electrodes in OFC across all 10 patients. Each color corresponds to a patient.

(B) Subjects (n = 10) chose between a sure prize and a risky gamble with varying probabilities for potential higher winnings. Trials resulted in a win if a second number was higher than the first. Gamble outcome was shown regardless of choice.

(C) Subjects' choices were significantly affected by likelihood of winning the gamble ($p < 0.001$; random effects logit analysis; error bars = SEM) and were comparable to those of healthy participants (gray line; all $p > 0.2$).

See also Figures S1 and S2 and Tables S1 and S2.

Because ECoG signals reflect cortical FP activity, one possibility is to analyze broadband activity using event-related potentials (ERPs) as in traditional EEG analyses [30, 31]. In contrast, motivated by recent human and animal findings, we focused on cortical HFA in the 70–200 Hz range, which is not observable in traditional scalp EEG due to distortions caused by signal propagation from the deep location of OFC and the reduced amplitude of HFA due to the 1/f power law. Growing evidence suggests that HFA acts as an index of local cortical computation [19, 32], unlike broadband power, which in addition reflects activity from coordinated interactions in broadly distributed networks [23, 33], and is better suited to reveal distinct computations across recording sites. Thus, we examined the extent to which variation in HFA power within and across trials was associated with reward-related signals (see Figure 2 for analytical strategy and example risk- and regret-encoding electrodes).

We applied this strategy to examine OFC-wide encoding across types of information and electrodes. Specifically, for each regressor of interest, we selected electrodes that showed a significant correlation ($p < 0.05$) at 5 or more consecutive time windows at any point (see STAR Methods) and averaged their temporal encoding profiles (%EV) to reveal OFC-wide encoding temporal profiles. Consistent with human neuroimaging and animal electrophysiological studies [4, 8, 14, 28, 34, 35], we found robust evidence within the HFA band for multiple valuation components related to choice (risk, gamble choice, offer value, and expected value of chosen option; see Figure S3 for additional risk analyses) and outcome (gamble win, gamble loss, RPE, and regret) processing.

In particular, choice and outcome processing signals were consistently time locked across multiple electrodes to external game presentation (Figures 3A and 3B) and outcome reveal (Figures 3C and 3D), respectively. The delays after the presentation of external information, game presentation and outcome reveal, respectively, were not statistically different (512.5 ± 59 ms and 287 ± 114.33 ms; $p = 0.14$; t test), with transient activation profiles of comparable duration (612.15 ± 132.9 ms and 712.5 ± 112.5 ms, respectively; $p = 0.58$; t test). The increase in overall variance for each information type was furthermore accompanied by an increase in the number of encoding electrodes (Figure 3). These results were robust to additional analyses more explicitly accounting for inter-subject or inter-electrode variability, and similar patterns were not observed when we used motor responses, i.e., left or right response, as a negative control (Figure S3).

In comparison, there was much weaker evidence of encoding in broadband power (Figure S4). Across all regressors, the proportion of encoding electrodes identified using HFA was significantly greater than using FP (mean HFA = 20.9% versus FP = 3.3%; $p < 10^{-5}$; t test). In addition, overall power modulation across OFC was maximal at the time of button press but weak at the times of maximal HFA encoding (i.e., ~750 ms post-outcome reveal for outcome regressors; Figure S4), strongly suggesting that HFA activity and encoding is temporally distinct from broadband power modulation.

Dissociable OFC Encoding of Past Choice and Outcome Information

In addition to reward-related signals relating to choice processes, we found that HFA signals also responded to a variety of past-trial characteristics [36, 37]. Specifically, we regressed HFA power on time-shifted choice and outcome regressors reflecting the characteristics of previous rounds (e.g., past loss indicates a gamble loss in the immediately preceding round). Because of the stationary nature of our task where probabilities are explicit and underlying distribution does not change over time, past and current regressors were uncorrelated (mean $R^2 = 2.1\%$; max $R^2 = 3.7\%$), thus allowing us to identify the extent to which neural signals reflected past trial information independently of current trial information. We found that past round

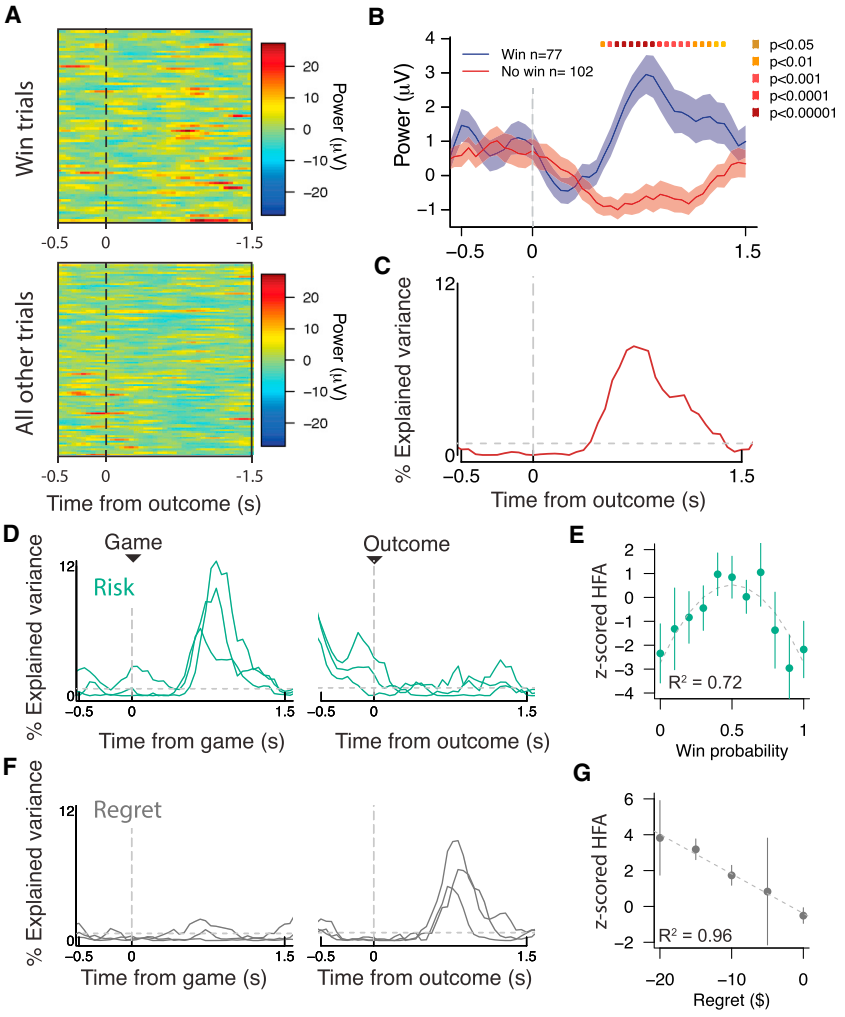

Figure 2. Analytical Approach and Example Encoding Electrodes

Electrode HFA time series was parsed into choice- and outcome-related epochs, and the inter-trial correlation between the HFA analytical amplitude and regressors of interest across task time was taken as an indication of encoding strength.

(A) HFA trials from example electrode encoding win information. Trials are time locked to gamble outcome reveal (t = 0) and split according to whether they resulted in a win (top) or not (bottom).

(B) Average HFA power for all win (blue trace; shade = SEM) and no win (red trace and shading) trials depicted in (A).

(C) Percentage of variance in the HFA signal in (A) and (B) explained by win or no win regressor (%EV).

(D) Three example electrodes encoding risk information. Activity is time locked to the time of initial game presentation (i.e., the deliberation period; left) and choice or outcome (right) and is expressed (as in D) as the percentage of variance in the HFA signal accounted for by risk information (%EV, linear regression; see STAR Methods).

(E) Relationship between win probability and HFA for one of the example electrodes at the time of peak encoding. The relationship follows an inverted u shape with win probabilities as would be expected for risk encoding.

(F) Three example electrodes, as in (D), but encoding regret information.

(G) As in (E), but showing a linear drop for electrodes encoding regret (parametrized as the extra payoff that would have been obtained by making a different choice).

See also Figures S4 and S6.

features were widely represented across the OFC, with the exception of past risk, and were dissociable from current choice and outcome signals (Figures 4A–4D; see Figure S5 for individual electrode examples).

Unlike transient choice and outcome signals, which were time locked to gamble and outcome reveal events, respectively, signals containing past trial information were sustained, with a longer encoding duration (Figure 5). Comparing the longest continuous stretch of time where HFA showed a significant association with each regressor of interest for all active electrodes, both past outcome (average duration = 1,341.37 ± 49.63 ms) and past choice (1,169.15 ± 61.2 ms) showed significantly more sustained activation than current choice and outcome signals (799.6 ± 36.94 and 706.9 ± 30.56 ms, respectively; all $p < 10^{-6}$; t test). As in the case of present information signals, this encoding was sustained through an increase in the number of encoding electrodes, and there was significantly less evidence of encoding at the level of broadband activity (Figure S4).

Interestingly, past trial characteristics were represented in spite of the fact that they did not appear to influence behavior. Random effects logistic regression showed that none of the past trial characteristics significantly affected risk-taking behavior (all $p > 0.15$). Moreover, evidence of such encoding appeared to be limited to the immediately preceding trial and not more temporally distant events. Specifically, we extended our time-lagged regressors to the past 5 trials (t_{-2} through t_{-5}). Strikingly, we found no evidence for encoding of information from earlier rounds (t_{-2}–t_{-5}; Figure 6A; see Figure 6B for individual regressors and Figure S5 for an in-depth comparison). That is, in contrast to predictions from associative learning accounts where learning signals contain the cumulative history of past outcomes, representation of past choices and outcomes in our data was short lived.

To assess the robustness of these and earlier results, we conducted several additional sets of analyses to address potential issues arising from multiple comparisons. First, to account for inter-subject or inter-electrode variation in neural activity, we ran a series of nested mixed-effects models, including patient and electrode identity as random effects to examine the impact of regressors on HFA activity. We found that all of our regressors were significantly active (all $p < 10^{-4}$; Bonferroni corrected), indicating that the computations were robust across electrodes and patients. To further verify that our results were not driven by regressor collinearity, we examined regressor correlation (Figure S6) and carried out a stepwise regression analysis, in which only regressors that significantly improve model fit are included in the results (STAR Methods). Overall, the stepwise regression

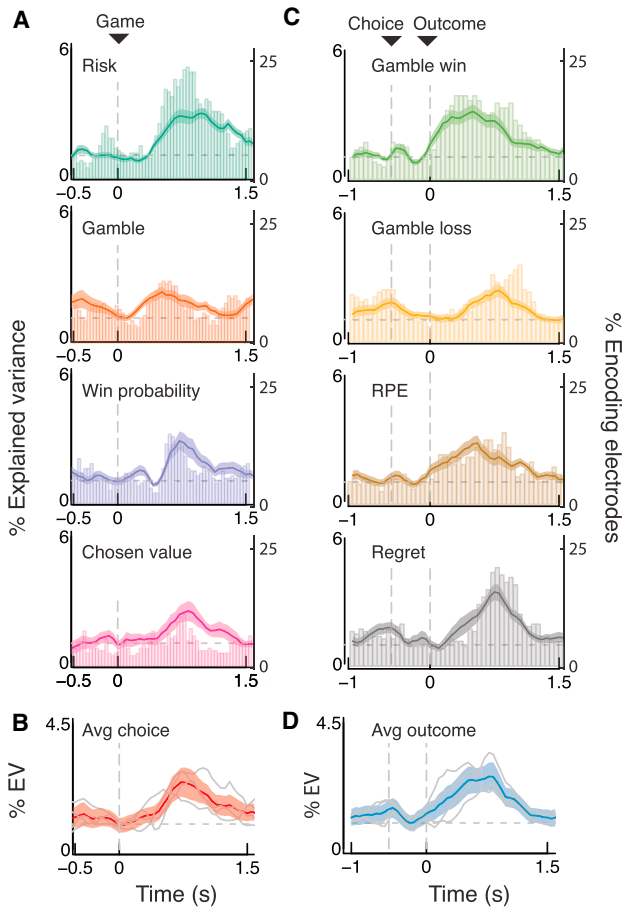

Figure 3. Human OFC Encodes Present Choice and Outcome Information

(A) Average % explained variance (%EV) (line plots and left axis; shade = SEM) and % of encoding electrodes (bars and right axis) time courses for linear regression of HFA neural activity onto all choice regressors (risk, gamble/safe bet choice, offer value, and expected chosen value) time locked to game presentation (t = 0); horizontal dotted line indicates chance results.

(B) Superimposed and average time courses for choice regressors; each gray line represents the average %EV shown for each regressor in (A).

(C) As in (A), but for outcome regressors (gamble win, gamble loss, reward prediction error [RPE], and regret), time locked to gamble outcome (t = 0).

(D) As in (B), but for outcome regressors (gamble win, gamble loss, RPE, and regret), time locked to gamble outcome (t = 0).

See also Figures S3, S4, and S6.

showed comparable results to our linear regression approach (Figure S6), indicating that our results were not driven by collinearity effects.

Anatomical Distribution of Present and Past Valuation Signals

Finally, we examined the anatomical localization of the above signals by examining their location across Brodmann areas (BAs) using Freesurfer and anatomical atlases [38] (see STAR Methods). The majority of electrodes in our sample were located in putative BA 11 (n = 53 out of 192 total), 13 (n = 40/192), and 14 (n = 67/192), providing a rare opportunity to assess the involvement of human central OFC in economic decision making. We found that, consistent with findings in monkey neurophysiological studies that implicate regions in the monkey homolog of the human central and mid-OFC [9, 14], there was strong evidence for the presence of electrodes capturing each type of signal (present and past choice and outcome) across all three areas (Figures 7B–7E). We found a similar proportion of electrodes encoded each valuation signal type across regions (Figure S7).

We found no consistent evidence for differential encoding of individual valuation components across OFC subregions (BA 11/13/14), or across anatomical gradients (fronto-posterior or medio-lateral; STAR Methods). To further verify that our results were not driven primarily by a subset of subjects, we examined the extent to which each value's signals were represented across patients. We found that all signals were present in at least 6 of the 10 patients in our sample (mean = 7.41 ± 0.4; Table S2), suggesting that our findings are robust and similarly represented across individuals.

In addition, we examined the extent to which electrodes represented multiple types of information. Individual OFC neurons are known to be capable of encoding multiple kinds of reward-related information [14], but whether this multiplexing appears at the level of HFA activity in individual cortical sites is largely unknown. To address this question, we further examined the results of our stepwise regression analysis (STAR Methods). To minimize the number of sets, we pooled encoding electrodes into four separate groups, integrated by electrodes encoding choice, outcome, past choice, and past outcome. We observed significant overlap in electrode sets, with most electrodes (n = 132/192; 68.7%) encoding at least two types of signals and 15.6% of electrodes (n = 30/192) encoding all four (Figure 7F). Electrodes encoding both present and past information were slightly overrepresented (chi-square test; $p < 0.05$; Figure S7), although a substantial proportion of electrodes encoded only present or past information (Figure 7F). Therefore, encoding of past and present information showed distinct temporal profiles and appeared in only partially overlapping OFC networks.

DISCUSSION

Human OFC is involved in an array of cognitive processes necessary for goal-directed behavior [6, 10]. Neural activity in OFC has been shown to reflect a variety of valuation signals necessary for estimating the value of available options, with rich evidence from fMRI studies demonstrating the existence of multiple valuation-related signals in human OFC, including expected reward, risk, and learning signals [3, 4, 39]. Here, we add to this knowledge by (1) providing novel insights into nature of human OFC encoding and (2) shedding light on the relationship between past human and animal findings.

First, we show that electrophysiological HFA in the OFC indexes multiple valuation components to a greater extent than broadband metrics. Specifically, the fast activation dynamics of HFA revealed that these signals were organized into two dissociable types of signals, with different information content showing different time courses in partially overlapping but distinct OFC networks. Signals related to choice and outcome evaluation processes were sequentially encoded in fast, transient activation volleys (Figure 3), whereas information about

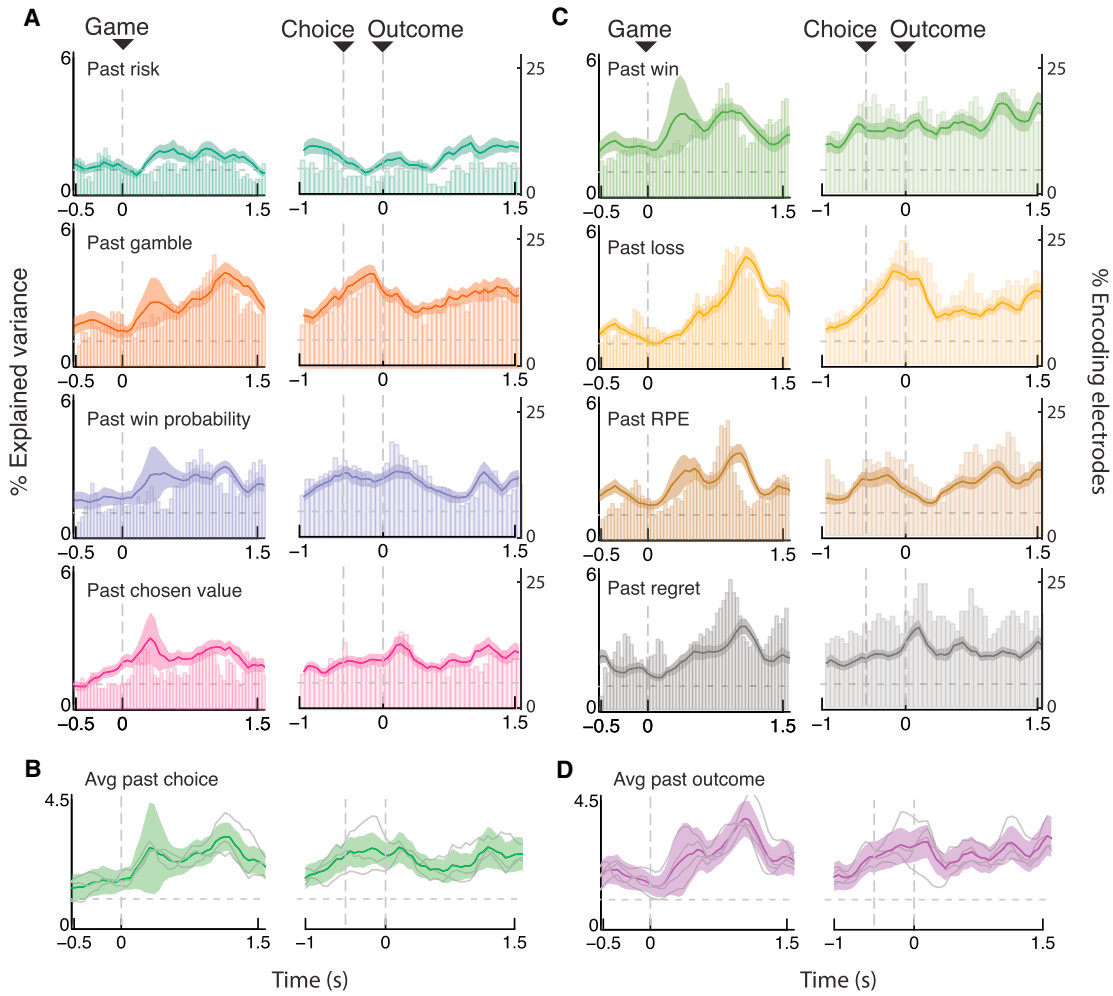

Figure 4. Human OFC Encodes Past Choice and Outcome Information from the Preceding Trial

(A) Average %EV (line plots and left axis; shade = SEM) and % of encoding electrodes (bars and right axis) time courses for linear regression of HFA neural activity onto all past choice regressors time locked to game (t = 0, left) and gamble outcome (t = 0, right); shade = SEM; horizontal dotted line indicates chance results.

(B) Superimposed and average time courses for past choice regressors, excluding past risk; each gray line represents the average %EV shown for each regressor in (A).

(C) As in (A), for past outcome regressors.

(D) As in (B), for past outcome regressors.

See also Figures S4, S5, and S6.

past choices and outcomes was represented in a second set of sustained signals overlapping both choice and outcome epochs (Figures 4 and 5) and were therefore encoded using a distinct temporal mechanism. The latter sustained signals, which have been shown in both rodent and monkey OFC [8, 14], were particularly notable in their information content: they reflect only what happened in the immediately preceding trial (e.g., whether subject chose to gamble, whether the gamble was won or lost, how much regret was experienced, etc.; Figure 6) rather than a cumulative history of past associations.

Thus, the timing and anatomical features of these signals add to our knowledge of human OFC functioning and go beyond predictions of influential theories based on associative learning models [35, 40, 41]. In particular, these models predict that past expectations and outcomes should be represented as an integrated learning signal with progressive decay of past information. Neural signatures of such a signal should therefore exhibit two properties. First, current and past outcomes should be present in the same signal rather than in separate electrodes following distinct temporal profiles. Second, the strengths of responses to past outcomes should depreciate smoothly, with distant past events showing progressively weaker representations compared to more recent events [42]. In contrast, we observed past and current signals, including responses reflecting reward prediction errors and regret, were represented in distinct networks of cortical sites (Figure 7) with a sharp intertemporal boundary between recent and distant past events (Figure 6).

Instead, our results are more compatible with the broader view of OFC functioning put forward in the more recent animal

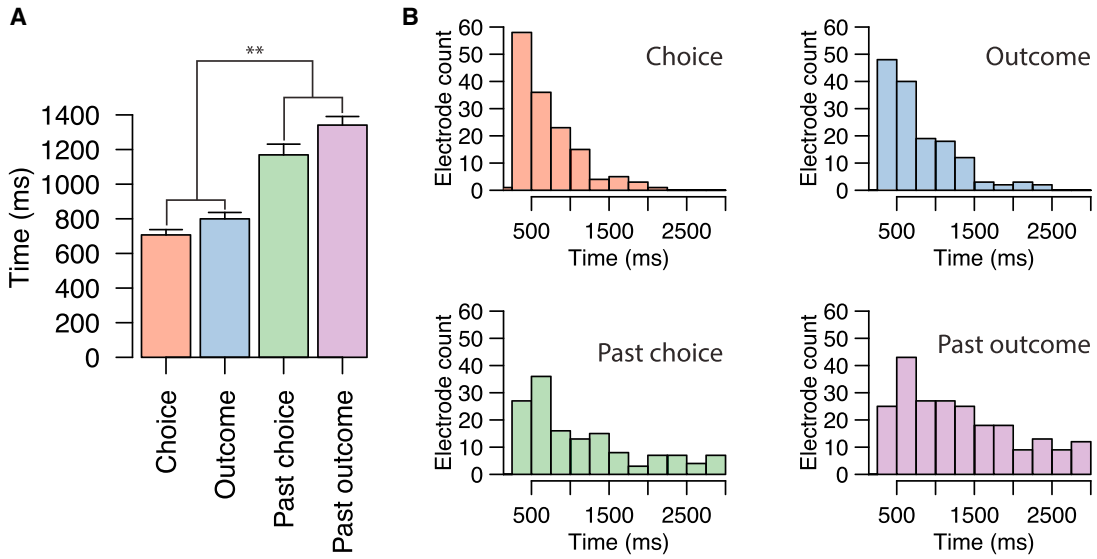

Figure 5. Dissociable Time Courses Representing Current and Past Information

(A) Mean duration of encoding across electrodes for each type of information (choice/outcome or past choice or past outcome). Choice groups include risk, gamble, offer value, and expected chosen value regressors (present/past); outcome groups include win, loss, RPE, and regret regressors (present/past). Duration of encoding was significantly longer for past than present valuation signals (**$p < 0.01$; t test; error bars = SEM).

(B) Histograms representing the distribution of encoding duration for individual electrodes. Each plot represents the duration of encoding for individual electrodes for all regressors in each group; data are the same as in (A).

literature centered on temporary maintenance and manipulation of goals and outcomes useful for behavioral performance [7]. The diverse encoding of past information is consistent with the view that OFC encodes a collection of relevant task states that includes not only information tied to external stimuli, such as the probability of winning the gamble, but also internal information that is not available in the environment and must be retained in memory, such as the previous action and outcome [7]. In particular, the sustained nature of our past encoding is consistent with proposals that OFC supports a working memory mechanism specialized for reward-related information [6], such that the OFC operates in a fashion similar to other prefrontal areas by holding relevant recent past information in working memory for short periods of time [43].

These ideas provide one possible explanation for the encoding of past choice and outcome information in our data, even as they do not appear to bias behavior. Under this proposal, past information may be maintained in working memory due to its potential usefulness for subsequent both action selection and value updating processes [5, 6, 9]. Although optimal decisions in our task should not incorporate past information, given the independent trial structure, it may nevertheless be beneficial for the brain to represent past history to detect any changes in the task environment, such as reversals, should they occur. Alternatively, the absence of signals integrating an extended history of trials may be due to the fact that our task did not require learning and that the nature of this signal may depend on whether paradigms require information to be accumulated across trials. Finally, it is possible that the functions of these signals were simply not captured in our behavioral assay. For example, past studies have suggested that OFC supports the representation of the hedonic value of temporally extended experiences [44], for example, what is colloquially referred to as "happiness." Thus, even if past choices and outcomes do not bias overt choice behavior in our task, they could be important for processes that update organisms' internal states. Future studies that manipulate learning, as well as expanding the set of behavioral assays, will be necessary to address these challenging questions.

In addition to variation in encoding duration, an important question remains regarding the extent to which there exists systematic variation in the relative onset of individual computational components. However, our ability to make conclusions about onset differences was limited by both the size of our data as well as between-subject variation. Although our dataset is large by human intracranial recording standards, the number of trials ($n = 200$) from each subject is small compared to animal studies that involve a small number of subjects but a much larger number of observations.

Our results also provide evidence regarding the anatomical organization of reward-related computations in the human brain. Whereas neurophysiological studies in monkeys have mostly implicated central OFC, corresponding to Brodmann areas 11 and 13 [14, 34], human fMRI studies commonly report vmPFC activations, corresponding to area 14 [5, 15, 35]. One possible explanation is that these differences reflect inter-species differences between humans and nonhuman primates. However, given the evidence for homology between monkey and human OFC [16], alternative explanations have focused on methodological differences between human and monkey studies, including (1) loss of OFC signal in fMRI due to susceptibility gradients above the orbital air-tissue interface [17, 18], (2) overtraining in animal studies, which often involve thousands of training trials over the course of months [8, 9, 14], and (3) the use of verbal

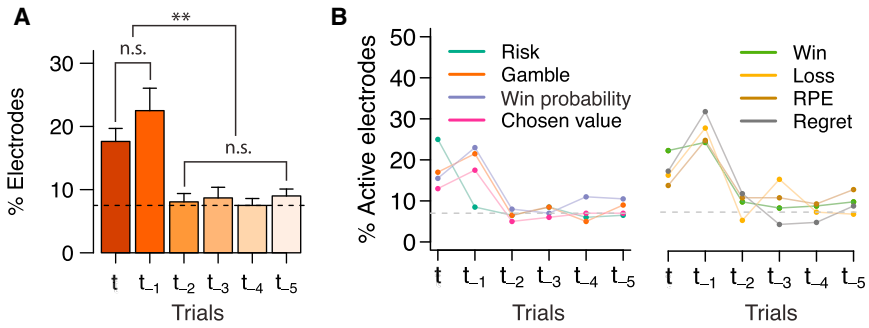

Figure 6. Past Representations Are Short Lived

(A) Significantly lower proportion of electrodes encoding distant (2–5 trials back; t_{-2} through t_{-5}) past choices and outcomes compared to present (t) and immediate past (previous trial, t_{-1}; **$p < 0.01$; t test; error bars = SEM).

(B) Proportion of electrodes encoding present and past information, separated by regressor: choice (left) and outcome (right) regressors. Horizontal dotted line indicates Null regressor results.

See also Figure S5.

instructions in human studies. Our electrophysiological recordings showing abundant encoding of value-related activations in central human OFC, including areas 11, 13, and 14 across multiple electrodes, participants, and types of valuation components, support the proposal that signal dropout in fMRI is a likely contributor to the lack of reported activation in human Brodmann areas 11 and 13.

By analyzing field potentials in the human OFC, our results provide a level of description complementary to the rich human BOLD [3–5, 11] and animal single unit [2, 8, 9, 14] literatures on the neural substrates of decision making. First, our time frequency analyses reveal that HFA are a more sensitive measure of reward-related responses than broadband FP activity. This is consistent with previous observations on the relationship between single-unit spiking, HFA, and BOLD. In particular, although broadband local field potential (LFP) activity is known to be correlated with both BOLD and single-unit spiking [45–47], these associations appear driven by activity in higher frequency bands. Specifically, power modulation in higher frequencies (40–130 Hz) has been shown to be significantly better at explaining BOLD responses than activity in lower frequencies, which are instead thought to reflect activity in broadly distributed networks [45, 48, 49]. Indeed, experiments in nonhuman primates, which do not face the same time constraints as our human intracranial recordings, have shown the existence of reward-related information in OFC LFP at the level of ERPs [50].

Similarly, HFA as captured using ECoG has been shown to be a better measure of neuronal spiking than broadband LFPs [46, 47], consistent with the idea that HFA reflects aggregate local neuronal output [19]. In contrast, due to challenges associated with conducting filtering and source spread, frequency-band-specific analyses using non-invasive recording techniques, such as EEG/MEG, have largely concentrated on the lower frequency bands, including low gamma band (50–60 Hz) [51]. Our observation that encoding is distributed across OFC also supports recent suggestions of intermingled, mixed selectivity in OFC [32]. Specifically, recent findings have shown that signals from multiple neurons with different encoding schemes [14] in the HFA signal do not result in weakening of encoding but rather generate comparably strong responses with clearer spatial and temporal structure [32]. Such functional grouping has been speculated to be computationally advantageous for decoding task-relevant information and for allowing behavioral flexibility [52].

As electrode locations were based solely on clinical criteria, variation in anatomical coverage can pose challenges for characterizing processing across brain regions. Within the OFC, a number of hypotheses have been proposed regarding functional differences across medial (area 14) and more lateral (areas 11 and 13) portions of OFC, including desirability (appetitive or aversive), primary or secondary nature of rewards, and processes (valuation or choice) [44, 53]. However, although we observed value-related signals across Brodmann areas 11, 13, and 14, there were no clear fronto-posterior or medio-lateral gradients for any of the reward-related computations we examined. Instead, we show that distinct types of signals are represented in overlapping but distinct cortical networks (Figure 7). A partial overlap provides a way in which a rich representation of task variables can be maintained in unique OFC sites, and sites that encode multiple types of signals provide a potential substrate for information integration. This distributed representation may be biased by the number of patients and electrodes in our sample. Alternatively, our data may reflect a distributed representation of distinct types of information across the orbital surface rather than anatomically clustered representations that can be uniquely captured by our multi-electrode ECoG approach. Consistent with this interpretation, distributed activation patterns have been observed in a number of cortical areas in ECoG studies [54, 55].

As with other studies involving rare patient populations, important methodological and interpretational limitations exist. First, there may be concerns regarding the generalizability of both neural activity and behavior of our patient participants to the general population. To address potential abnormalities in neural activity, we undertook extensive efforts to only test patients fully alert and cooperative and removed from analysis electrodes placed over seizure foci or abnormal tissue (see STAR Methods). Behaviorally, we addressed potential fatigue issues and the strict time limits of our recording sessions by minimizing the cognitive complexity of the task. Indeed, we found that behavioral performance of patients was consistent with those from healthy participants (Figure 1C), suggesting that key circuits implicated in decision making under uncertainty are intact in our patient sample.

Finally, although ECoG is not affected by air-tissue artifacts present in fMRI measures of OFC activity, there are concerns of signal contamination by adjacent extra-ocular muscle movements that may have spectral characteristics similar to those of neural signals of interest. We were unable to record eye movement with our intracranial data and cannot rule out the existence of such artifacts in our data directly. However, prior findings incorporating eye movement data found no evidence for such artifacts in the OFC [56]. In addition, we examined whether

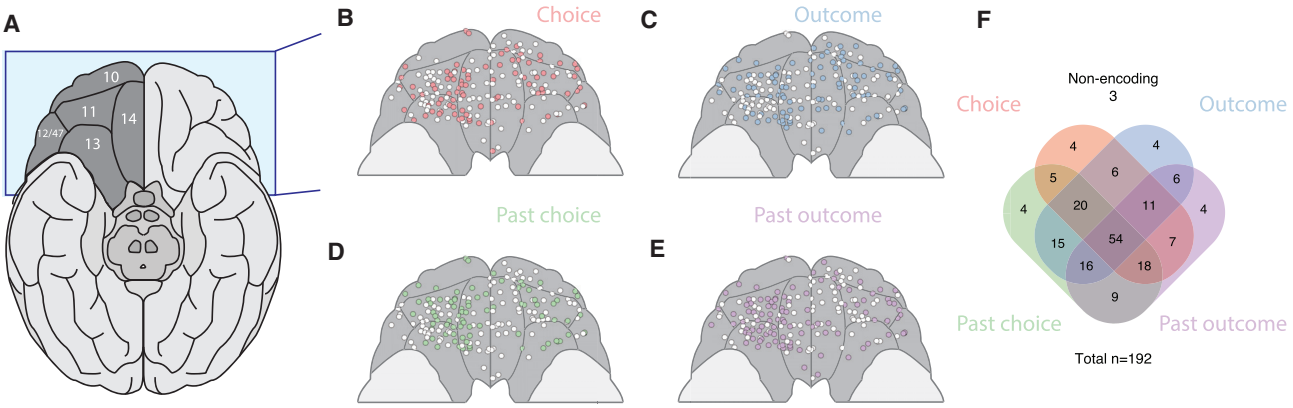

Figure 7. Anatomical Distribution of Valuation Components

(A) Ventral view of the brain. Blue shadowed area corresponds to OFC as shown in (B) and (E). Boundaries and white numbers (left) indicate putative Brodmann areas [6].

(B) Anatomical localization of electrodes encoding choice signals (red dots; white dots represent non-encoding electrodes).

(C–E) Same as (B) for electrodes encoding outcome (C), past choice (D), and past outcome (E) signals.

(F) Venn diagram indicating the number of electrodes (out of n = 192) encoding one or several types of signals.

movement-related activity was represented in OFC and found no significant association between the direction of movement (left-right) and HFA activity (Figure S3), suggesting that movement-related activity is not present in OFC HFA.

More generally, intracranial recording approaches open the door for human studies to build on insights from animal and neuroimaging research to study long-standing questions involving human OFC functioning, such as the interregional communication and flow of information across different brain regions [21, 23, 57]. For example, given their different information content, transient and sustained encoding modes may be related to their routes of entry into OFC such that the former signals reflect external input reaching OFC from ascending sensory pathways [58], and the latter signals reflect internal inputs relayed in a top-down manner from executive control and memory structures, such as lateral PFC or hippocampus [59]. Similarly, past fMRI studies have emphasized the importance of lateral PFC in controlling and biasing valuation signals in OFC during decision making [5], but the precise nature of the underlying mechanisms have remained unclear. Addressing these questions will help elucidate the neural basis of uniquely human decisions related to highly complex decisions, abstract rewards, or those performed in complex social settings.

STAR★METHODS

Detailed methods are provided in the online version of this paper and include the following:

- KEY RESOURCES TABLE
- CONTACT FOR REAGENT AND RESOURCE SHARING
- EXPERIMENTAL MODEL AND SUBJECT DETAILS
  - Subjects
- METHOD DETAILS
  - Behavioral task
  - ECoG Recording
  - Anatomical reconstructions
  - Behavioral Analysis
- QUANTIFICATION AND STATISTICAL ANALYSIS
  - ECoG analysis and behavioral regression
  - Stepwise regression
- DATA AND SOFTWARE AVAILABILITY

SUPPLEMENTAL INFORMATION

Supplemental Information includes seven figures and two tables and can be found with this article online at https://doi.org/10.1016/j.cub.2018.07.045.

ACKNOWLEDGMENTS

We would like to thank the patient volunteers and the research and surgical staff at the recording sites for their support and cooperation, members of the Knight lab for assistance with data collection, and Joni Wallis and Xinying Cai for useful discussion. This project was supported by National Institute of Neurological Disorders and Stroke (NINDS) R37NS21135; Defense Advanced Research Projects Agency; Systems-Based Neurotechnology for Emerging Therapies, University of California (DARPA SUBNETS UC) (to R.T.K.); and National Institute of Mental Health (NIMH) MH098023 (to M.H.), NIMH K01MH108815 (to I.S.), and R21MH109851 (to R.T.K., M.H., and I.S.). Electrophysiological and behavioral data are archived at the Collaborative Research in Computational Neuroscience (CRCNS) center at the University of California, Berkeley.

AUTHOR CONTRIBUTIONS

I.S., M.H., and R.T.K. designed research; I.S. and M.H. designed the gambling task; I.S. collected the data; J.L., E.C., J.P., and G.S. provided access and guidance in data acquisition from the patients; I.S. and M.H. analyzed the data, with assistance from A.S. on anatomical reconstructions; and I.S., M.H., and R.T.K. interpreted the data and wrote the manuscript.

DECLARATION OF INTERESTS

The authors declare no competing interests.

Received: April 6, 2018
Revised: June 22, 2018
Accepted: July 16, 2018
Published: September 13, 2018

REFERENCES

1. Rangel, A., Camerer, C., and Montague, P.R. (2008). A framework for studying the neurobiology of value-based decision making. Nat. Rev. Neurosci. *9*, 545–556.
2. Schultz, W., Dayan, P., and Montague, P.R. (1997). A neural substrate of prediction and reward. Science *275*, 1593–1599.
3. Gottfried, J.A., O'Doherty, J., and Dolan, R.J. (2003). Encoding predictive reward value in human amygdala and orbitofrontal cortex. Science *301*, 1104–1107.
4. Hsu, M., Bhatt, M., Adolphs, R., Tranel, D., and Camerer, C.F. (2005). Neural systems responding to degrees of uncertainty in human decision-making. Science *310*, 1680–1683.
5. Hare, T.A., Camerer, C.F., and Rangel, A. (2009). Self-control in decision-making involves modulation of the vmPFC valuation system. Science *324*, 646–648.
6. Wallis, J.D. (2007). Orbitofrontal cortex and its contribution to decision-making. Annu. Rev. Neurosci. *30*, 31–56.
7. Wilson, R.C., Takahashi, Y.K., Schoenbaum, G., and Niv, Y. (2014). Orbitofrontal cortex as a cognitive map of task space. Neuron *81*, 267–279.
8. Sul, J.H., Kim, H., Huh, N., Lee, D., and Jung, M.W. (2010). Distinct roles of rodent orbitofrontal and medial prefrontal cortex in decision making. Neuron *66*, 449–460.
9. Padoa-Schioppa, C., and Assad, J.A. (2006). Neurons in the orbitofrontal cortex encode economic value. Nature *441*, 223–226.
10. Rushworth, M.F.S., Noonan, M.P., Boorman, E.D., Walton, M.E., and Behrens, T.E. (2011). Frontal cortex and reward-guided learning and decision-making. Neuron *70*, 1054–1069.
11. Tom, S.M., Fox, C.R., Trepel, C., and Poldrack, R.A. (2007). The neural basis of loss aversion in decision-making under risk. Science *315*, 515–518.
12. Coricelli, G., Critchley, H.D., Joffily, M., O'Doherty, J.P., Sirigu, A., and Dolan, R.J. (2005). Regret and its avoidance: a neuroimaging study of choice behavior. Nat. Neurosci. *8*, 1255–1262.
13. Tremblay, L., and Schultz, W. (1999). Relative reward preference in primate orbitofrontal cortex. Nature *398*, 704–708.
14. Kennerley, S.W., Behrens, T.E.J., and Wallis, J.D. (2011). Double dissociation of value computations in orbitofrontal and anterior cingulate neurons. Nat. Neurosci. *14*, 1581–1589.
15. Kable, J.W., and Glimcher, P.W. (2007). The neural correlates of subjective value during intertemporal choice. Nat. Neurosci. *10*, 1625–1633.
16. Wallis, J.D. (2011). Cross-species studies of orbitofrontal cortex and value-based decision-making. Nat. Neurosci. *15*, 13–19.
17. Stenger, V.A. (2006). Technical considerations for BOLD fMRI of the orbitofrontal cortex. In The Orbitofrontal Cortex, D. Zald, and S. Rauch, eds. (Oxford), pp. 423–446.
18. Deichmann, R., Gottfried, J.A., Hutton, C., and Turner, R. (2003). Optimized EPI for fMRI studies of the orbitofrontal cortex. Neuroimage *19*, 430–441.
19. Buzsáki, G., Anastassiou, C.A., and Koch, C. (2012). The origin of extracellular fields and currents–EEG, ECoG, LFP and spikes. Nat. Rev. Neurosci. *13*, 407–420.
20. Mesgarani, N., Cheung, C., Johnson, K., and Chang, E.F. (2014). Phonetic feature encoding in human superior temporal gyrus. Science *343*, 1006–1010.
21. Canolty, R.T., Edwards, E., Dalal, S.S., Soltani, M., Nagarajan, S.S., Kirsch, H.E., Berger, M.S., Barbaro, N.M., and Knight, R.T. (2006). High gamma power is phase-locked to theta oscillations in human neocortex. Science *313*, 1626–1628.
22. Voytek, B., Kayser, A.S., Badre, D., Fegen, D., Chang, E.F., Crone, N.E., Parvizi, J., Knight, R.T., and D'Esposito, M. (2015). Oscillatory dynamics coordinating human frontal networks in support of goal maintenance. Nat. Neurosci. *18*, 1318–1324.
23. Buzsáki, G., and Draguhn, A. (2004). Neuronal oscillations in cortical networks. Science *304*, 1926–1929.
24. Edwards, E., Soltani, M., Deouell, L.Y., Berger, M.S., and Knight, R.T. (2005). High gamma activity in response to deviant auditory stimuli recorded directly from human cortex. J. Neurophysiol. *94*, 4269–4280.
25. Ray, S., Niebur, E., Hsiao, S.S., Sinai, A., and Crone, N.E. (2008). High-frequency gamma activity (80-150Hz) is increased in human cortex during selective attention. Clin. Neurophysiol. *119*, 116–133.
26. Lachaux, J.-P., Axmacher, N., Mormann, F., Halgren, E., and Crone, N.E. (2012). High-frequency neural activity and human cognition: past, present and possible future of intracranial EEG research. Prog. Neurobiol. *98*, 279–301.
27. Cohen, M.X., Axmacher, N., Lenartz, D., Elger, C.E., Sturm, V., and Schlaepfer, T.E. (2009). Good vibrations: cross-frequency coupling in the human nucleus accumbens during reward processing. J. Cogn. Neurosci. *21*, 875–889.
28. Li, Y., Vanni-Mercier, G., Isnard, J., Mauguière, F., and Dreher, J.-C. (2016). The neural dynamics of reward value and risk coding in the human orbitofrontal cortex. Brain *139*, 1295–1309.
29. Preuschoff, K., Bossaerts, P., and Quartz, S.R. (2006). Neural differentiation of expected reward and risk in human subcortical structures. Neuron *51*, 381–390.
30. Holroyd, C.B., Nieuwenhuis, S., Yeung, N., and Cohen, J.D. (2003). Errors in reward prediction are reflected in the event-related brain potential. Neuroreport *14*, 2481–2484.
31. Gehring, W.J., and Willoughby, A.R. (2002). The medial frontal cortex and the rapid processing of monetary gains and losses. Science *295*, 2279–2282.
32. Rich, E.L., and Wallis, J.D. (2017). Spatiotemporal dynamics of information encoding revealed in orbitofrontal high-gamma. Nat. Commun. *8*, 1139.
33. Fujisawa, S., and Buzsáki, G. (2011). A 4 Hz oscillation adaptively synchronizes prefrontal, VTA, and hippocampal activities. Neuron *72*, 153–165.
34. O'Neill, M., and Schultz, W. (2010). Coding of reward risk by orbitofrontal neurons is mostly distinct from coding of reward value. Neuron *68*, 789–800.
35. Daw, N.D., Gershman, S.J., Seymour, B., Dayan, P., and Dolan, R.J. (2011). Model-based influences on humans' choices and striatal prediction errors. Neuron *69*, 1204–1215.
36. Gottfried, J.A., O'Doherty, J., and Dolan, R.J. (2002). Appetitive and aversive olfactory learning in humans studied using event-related functional magnetic resonance imaging. J. Neurosci. *22*, 10829–10837.
37. O'Doherty, J.P. (2004). Reward representations and reward-related learning in the human brain: insights from neuroimaging. Curr. Opin. Neurobiol. *14*, 769–776.
38. Stolk, A., Griffin, S., van der Meij, R., Dewar, C., Sáez, I., Lin, J.J., Piantoni, G., Schoffelen, J.-M., Knight, R.T., and Oostenveld, R. (2018). Integrated analysis of anatomical and electrophysiological human intracranial data. Nat. Protoc. Published online July 9, 2018. https://doi.org/10.1038/s41596-018-0009-6.
39. Camille, N., Coricelli, G., Sallet, J., Pradat-Diehl, P., Duhamel, J.-R., and Sirigu, A. (2004). The involvement of the orbitofrontal cortex in the experience of regret. Science *304*, 1167–1170.
40. Gläscher, J., Daw, N., Dayan, P., and O'Doherty, J.P. (2010). States versus rewards: dissociable neural prediction error signals underlying model-based and model-free reinforcement learning. Neuron *66*, 585–595.
41. Schoenbaum, G., and Roesch, M. (2005). Orbitofrontal cortex, associative learning, and expectancies. Neuron *47*, 633–636.
42. Sutton, R.S., and Barto, A.G. (1998). Reinforcement Learning: An Introduction (Cambridge University Press).
43. Curtis, C.E., and D'Esposito, M. (2003). Persistent activity in the prefrontal cortex during working memory. Trends Cogn. Sci. *7*, 415–423.

44. Rudebeck, P.H., and Murray, E.A. (2014). The orbitofrontal oracle: cortical mechanisms for the prediction and evaluation of specific behavioral outcomes. Neuron *84*, 1143–1156.

45. Logothetis, N.K., Pauls, J., Augath, M., Trinath, T., and Oeltermann, A. (2001). Neurophysiological investigation of the basis of the fMRI signal. Nature *412*, 150–157.

46. Berens, P., Keliris, G.A., Ecker, A.S., Logothetis, N.K., and Tolias, A.S. (2008). Feature selectivity of the gamma-band of the local field potential in primate primary visual cortex. Front. Neurosci. *2*, 199–207.

47. Liu, J., and Newsome, W.T. (2006). Local field potential in cortical area MT: stimulus tuning and behavioral correlations. J. Neurosci. *26*, 7779–7790.

48. Mukamel, R., Gelbard, H., Arieli, A., Hasson, U., Fried, I., and Malach, R. (2005). Coupling between neuronal firing, field potentials, and FMRI in human auditory cortex. Science *309*, 951–954.

49. Nir, Y., Fisch, L., Mukamel, R., Gelbard-Sagiv, H., Arieli, A., Fried, I., and Malach, R. (2007). Coupling between neuronal firing rate, gamma LFP, and BOLD fMRI is related to interneuronal correlations. Curr. Biol. *17*, 1275–1285.

50. Hunt, L.T., Behrens, T.E., Hosokawa, T., Wallis, J.D., and Kennerley, S.W. (2015). Capturing the temporal evolution of choice across prefrontal cortex. eLife *4*, e11945.

51. Polanía, R., Krajbich, I., Grueschow, M., and Ruff, C.C. (2014). Neural oscillations and synchronization differentially support evidence accumulation in perceptual and value-based decision making. Neuron *82*, 709–720.

52. Rigotti, M., Barak, O., Warden, M.R., Wang, X.-J., Daw, N.D., Miller, E.K., and Fusi, S. (2013). The importance of mixed selectivity in complex cognitive tasks. Nature *497*, 585–590.

53. O'Doherty, J., Kringelbach, M.L., Rolls, E.T., Hornak, J., and Andrews, C. (2001). Abstract reward and punishment representations in the human orbitofrontal cortex. Nat. Neurosci. *4*, 95–102.

54. Gonzalez, A., Hutchinson, J.B., Uncapher, M.R., Chen, J., LaRocque, K.F., Foster, B.L., Rangarajan, V., Parvizi, J., and Wagner, A.D. (2015). Electrocorticography reveals the temporal dynamics of posterior parietal cortical activity during recognition memory decisions. Proc. Natl. Acad. Sci. USA *112*, 11066–11071.

55. Haller, M., Case, J., Crone, N.E., Chang, E.F., King-Stephens, D., Laxer, K.D., Weber, P.B., Parvizi, J., Knight, R.T., and Shestyuk, A.Y. (2018). Persistent neuronal activity in human prefrontal cortex links perception and action. Nat. Hum. Behav. *2*, 80–91.

56. Jerbi, K., Freyermuth, S., Dalal, S., Kahane, P., Bertrand, O., Berthoz, A., and Lachaux, J.-P. (2009). Saccade related gamma-band activity in intracerebral EEG: dissociating neural from ocular muscle activity. Brain Topogr. *22*, 18–23.

57. Buschman, T.J., Denovellis, E.L., Diogo, C., Bullock, D., and Miller, E.K. (2012). Synchronous oscillatory neural ensembles for rules in the prefrontal cortex. Neuron *76*, 838–846.

58. Ongür, D., An, X., and Price, J.L. (1998). Prefrontal cortical projections to the hypothalamus in macaque monkeys. J. Comp. Neurol. *401*, 480–505.

59. Carmichael, S.T., and Price, J.L. (1995). Limbic connections of the orbital and medial prefrontal cortex in macaque monkeys. J. Comp. Neurol. *363*, 615–641.

STAR★METHODS

KEY RESOURCES TABLE

REAGENT or RESOURCE	SOURCE	IDENTIFIER
Deposited Data		
Electrophysiological and behavioral data	This paper	https://crcns.org/data-sets/ofc/ofc-3
Software and Algorithms		
MATLAB R2016b	Mathworks software	RRID: SCR:001622
RStudio running R v.3.4.1	R Foundation for Statistical Computing	RRID: SCR:000432

CONTACT FOR REAGENT AND RESOURCE SHARING

Further information and requests for resources should be directed to and will be fulfilled by the Lead Contact, Ming Hsu (mhsu@haas.berkeley.edu).

EXPERIMENTAL MODEL AND SUBJECT DETAILS

Subjects

Data was collected from 10 (4 female) adult subjects with intractable epilepsy who were implanted with chronic subdural grid and/or strip electrodes as part of a pre-operative procedure to localize the epileptogenic focus. We paid careful attention to the patient's neurological condition and only tested when the patient was fully alert and cooperative. The surgeons determined electrode placement and treatment based solely on the clinical needs of each patient. Patient recordings took place at four hospitals: the University of California, San Francisco (UCSF) Hospital (n = 2), the Stanford School of Medicine (n = 2), the University of California, Irvine Medical Center (UCI) (n = 5) and at Albany Medical College (n = 1). Due to IRB limitations, subjects were not paid for their participation in the study but were encouraged to make as many points as possible. As part of the clinical observation procedure, patients were off antiepileptic medication during these experiments. Healthy participants (n = 10) with no prior history of neurological disease were recruited from UC Berkeley's undergraduate population and played an identical version of the gambling task. All subjects gave written informed consent to participate in the study in accordance with the University of California, Berkeley Institutional Review Board.

METHOD DETAILS

Behavioral task

We probed risk-reward tradeoffs using a simple gambling task in which subjects chose between a sure payoff and a gamble for potential higher winnings. Trials started with a fixation cross (t = 0), followed by the game presentation screen (t = 750ms). At that time, patients were given up to 2 s to choose between a fixed prize (safe bet, $10) and a higher payoff gamble (e.g., $30; Figure 1). Gamble prizes varied between $10 and $30, in $5 increments. If the patient did not choose within the allotted time limit, a timeout occurred and no reward was awarded for that round. Timeouts were infrequent (9.98% of all trials) and were excluded from analysis. Gamble win probability varied round by round; at the time of game presentation, subjects are shown a number between 0-10. At the time of outcome (t = 550ms post-choice), a second number (also 0-10) is revealed, and the subject wins the prize if the second number is greater than the first one. Only integers were presented, and ties were not allowed; therefore, a shown '2′ had a win probability of 20%. The delay between buttonpress and gamble outcome presentation (550ms) was fixed, and activity for both epochs is temporally aligned. Therefore, offer value, risk and chosen value vary parametrically on a round-by-round basis, and patients had full knowledge of the (fair) task structure from the beginning of the game. Both numbers were randomly generated using a uniform distribution. The gamble outcome (win/loss) was revealed regardless of subject choice, allowing us to calculate experiential and counterfactual prediction errors (see Behavioral analysis, below). A new round started 1 s after outcome reveal. Patients played a total of 200 rounds (plus practice rounds), and a full experimental run typically lasted 12-15min. Location of safe bet and gamble options (left/right) was randomized across trials. Patients completed a training session prior to the game in which they played at least 10 rounds under the experimenter's supervision until they felt confident they understood the task, at which point they started the game. This gambling task minimized other cognitive demands (working memory, learning, etc.) on our participants, while at the same time allowing us to probe important decision-making components implicated in previous computational and empirical studies, such as expected reward, payoff risk, prediction errors, and counterfactual signals.

ECoG Recording

ECoG was recorded and stored with behavioral data. Data collection was carried out using Tucker-Davis Technologies (Albany, Stanford and UCSF) or Nihon-Kohden (at UCI) systems. Data processing was identical across all sites: channels were

amplified x10000, analog filtered (0.01-1000 Hz) with > 2kHz digitization rate, re-referenced to a common average offline, high-pass filtered at 1.0 Hz with a symmetrical (phase true) finite impulse response (FIR) filter (~35 dB/octave roll-off). Channels with low signal-to-noise ratio (SNR) were identified and deleted (i.e., 60 Hz line interference, electromagnetic equipment noise, amplifier saturation, poor contact with cortical surface). Out of 210 OFC electrodes, 192 were artifact-free and included in subsequent analyses. Additionally, all channels were visually inspected by a neurologist to exclude epochs of aberrant or noisy activity (typically < 1% of datapoints). A photodiode recorded screen updates in the behavioral task, recorded in the electrophysiological system as an analog input and used to synchronize behavioral and electrophysiological data. Data analysis was carried out in MATLAB and R using custom scripts. Data for each channel was downsampled to 1KHz and filtered into high frequency activity (HFA; 70–200 Hz) using a two-way, zero phase-lag, finite impulse response band pass filter to prevent phase distortion.

Anatomical reconstructions

For each patient, we collected a pre-operative anatomical MRI (T1) image and a post-implantation CT scan. The CT scan allows identification of individual electrodes but offers poor anatomical resolution, making it difficult to determine their anatomical location. Therefore, the CT scan was realigned to the pre-operative MRI scan. Briefly, both the MRI and CT images were aligned to a common coordinate system and fused with each other using a rigid body transformation. Following CT-MR co-registration, we compensated for brain shift, an inward sinking and shrinking of brain tissue caused by the implantation surgery. A hull of the patient brain was generated using the Freesurfer analysis suite, and each grid and strip was realigned independently onto the hull of the patient's brain. This step often avoided localization errors of several millimeters. Subsequently, each patient's brain and the corresponding electrode locations were normalized to a template using a volume-based normalization technique, and snapped to the cortical surface [38]. Finally, the electrode coordinates are cross-referenced with labeled anatomical atlases (JuBrain and AAL atlases) to obtain the gross anatomical location of the electrodes, verified by visual confirmation of electrode location based on surgical notes. Only electrodes confirmed to be in OFC (n = 192) were included in the analysis. For display purposes, electrodes are displayed over a traced reconstruction of the ventral surface showing putative Brodmann areas. For analysis of anatomical gradients of encoding, for every electrode/regressor combination we took the %EV at the time of average regressor encoding (i.e., at the maximum %EV in the average activation profile across electrodes) as an index of information encoding. We then carried out two different analyses: first, we compared the distribution of %EV values for each regressor across areas using a K-S test. Second, we examined whether a correlation existed between the %EV values and the fronto-posterior and medio-lateral location of individual electrodes (i.e., x and y coordinates in the anatomical reconstruction, referenced to the anterior commisure).

Behavioral Analysis

We derived round-to-round parametric signals from a value-based decision-making framework that includes notions of win probability, expected reward, reward-prediction errors and counterfactual errors (defined as the difference between actual reward and the maximum reward that could have been obtained, commonly described as "regret," in $) and risk, as well as binary classifications related to choice (gamble/safe bet) and outcome (gamble win, gamble loss; see Table S1 for a complete description). As an example, if a '2' is initially shown, in a $30 prize trial and the subject chose to gamble, win probability would be 0.8 (probability of obtaining a second number > 2), chosen value would be $24 ($30 × 0.8) and the binary gamble indicator would be 1. Risk is maximal at 0.5 win probability and lowest at $p_w = 0$ and $p_w = 1$, so in this example it would be low. If the gamble resulted in a loss, the RPE would be large and negative (-$24, the difference between the chosen value of $24 and the actual outcome, $0) and regret would be -$10 (the difference between the actual outcome, $0 and the counterfactual best possible outcome, the safe bet worth $10). Importantly, RPEs are zero in safe bet trials (the won amount is always as expected, $10), but regret may not be (i.e., "would have won"). To examine whether HFA captured information about past events, we built time-shifted versions of the regressors in our sample. We used the same parameterization as for current regressors, but derived using information from earlier trials (one trial back, t_{-1}, through 5 trials back, t_{-5}). For example, gamble t_{-3} indicates whether the subject chose to gamble 3 trials back. As for present regressors, % of active electrodes was calculated as the proportion that shows significant encoding (linear regression $p < 0.05$) for over 5 consecutive windows.

QUANTIFICATION AND STATISTICAL ANALYSIS

ECoG analysis and behavioral regression

To identify HFA encoding, we used a regression approach where the dependent variable was defined as the analytic amplitude of the HFA time series extracted via Hilbert transform. Next, we divided HFA time series into event-related epochs using a 200-ms baseline to remove any pre-stimulus differences in baseline amplitude, averaging HFA activity using a 200ms rolling window at 50ms increments. To identity task-selective channels, we performed separate linear regressions of average HFA activity on each reward-related regressor of interest. Given the inter-trial variability in response latencies, we performed this analysis separately for time-locked to both game presentation (game epoch) and to buttonpress/reward events (buttonpress epoch). Analyses to identify encoding in FPs followed a similar procedure, except replacing HFA with broadband power as the dependent variable.

We used the resulting R^2 (variance in the neural data that can be explained by the behavioral regressors of interest, % explained variance, %EV) as a metric of the quality of the fit. This approach is insensitive with respect to time of task-related activation and to the direction of encoding (i.e., HFA increases or decreases). Electrodes were classified as task active for any given regressor if they

showed a significant correlation ($p < 0.05$) at 5 or more consecutive time windows at any point during the epochs. False positive rate was determined using a permutation strategy. For each regressor-HFA regression, we shuffled the relationship between behavioral labels and HFA activity 1,000 times. The resulting distribution was taken as the null for that particular regressor-electrode combination. Duration of encoding in individual regressors/electrodes (Figure 5) was defined as the longest stretch of time in which all time points showed significant encoding ($p < 0.05$).

Stepwise regression

To verify the encoding profile of individual electrodes was not affected by regressor collinearity, we used a stepwise regression model successfully used in the analysis of single unit activity in similar settings in the past [9]. The analysis for each electrode proceeded as follows: first, we carried out multiple individual linear regressions for all regressors. To leverage the time profile of the signals without imposing restrictions on activation timing, an aggregate statistic was calculated as the sum of F-stats for the longest stretch of consecutive significant (linear regression $p < 0.05$) windows. We then repeated this procedure 10,000 times after shuffling the behavioral labels, and took the proportion of permuted fits with a sum-of-F-stat higher than that in the original dataset was taken as the permutation p value. This p value was further corrected for multiple comparisons using a Bonferroni correction (across $n = 192$ electrodes); regressors that did not survive multiple comparisons were discarded at this point.

Subsequently, we sought to identify the set of regressors that best explains neural HFA variance by performed a model selection procedure on the surviving regressor set. We first selected the regressor that explained the most variance in the neural data (maximum peak %EV) as the base model. We then created an alternative complex model by incorporating the second regressor that most improved the model. These two models were compared using an ANOVA test; if the complex model resulted in a significantly improved fit (ANOVA $p < 0.05$), we rejected the basic model. This process was iteratively repeated by adding new regressors, sorted by residual %EV improvement, until the model could not be further improved (ANOVA $p > 0.05$). Finally, we estimated the proportion of electrodes encoding each variable across all electrodes, regardless of the order in which they were incorporated into the model.

To verify that the results were not driven by inter-subject or inter-electrode variability, we conducted mixed-effects model analysis using the concatenated HFA for all electrodes as dependent variable, round-by-round regressors of interest (risk, regret, etc.) as fixed effects, and patient and electrode ID as nested mixed-effects.

DATA AND SOFTWARE AVAILABILITY

The accession number for the electrophysiological and behavioral data reported in this paper is CRCNS: K0VM49GF (https://doi.org/10.6080/K0VM49GF).

Current Biology, Volume *28*

Supplemental Information

Encoding of Multiple Reward-Related Computations in Transient and Sustained High-Frequency Activity in Human OFC

Ignacio Saez, Jack Lin, Arjen Stolk, Edward Chang, Josef Parvizi, Gerwin Schalk, Robert T. Knight, and Ming Hsu

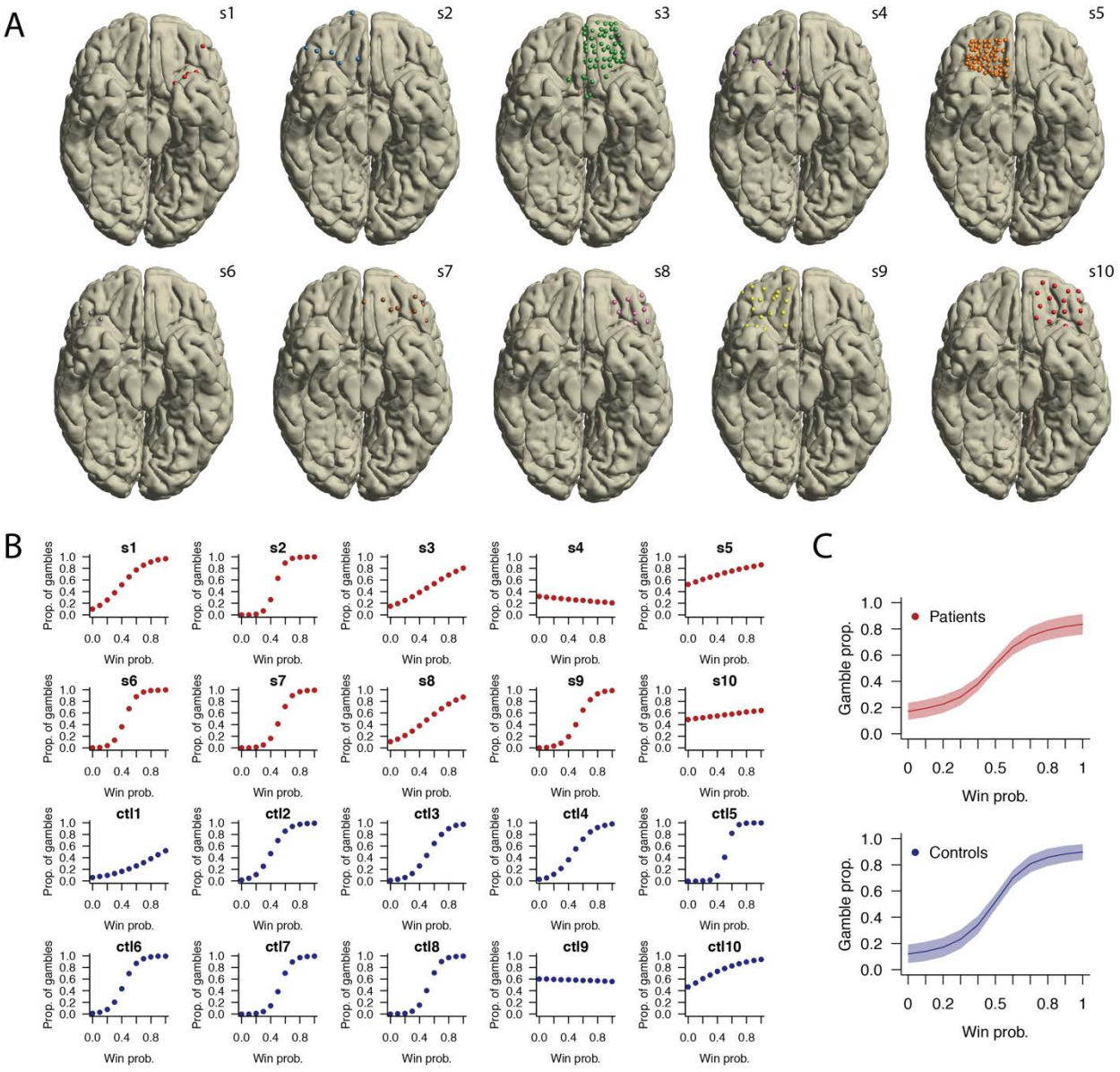

Figure S1. Individual anatomical coverage and behavior. Related to Figure 1. (A) Individual reconstruction of the 10 patients included in the study, showing location of all ECoG electrodes in the ventral surface of the brain for each individual patient (s1-s10). The final number of electrodes, after excluding those located outside of OFC and with aberrant activity, was 192. (B) Sigmoidal fits between proportion of gambles and game win probability for each of the 10 patient (top, red points) and each of the 10 control subjects (bottom, blue points). (C) Average and SEM (colored line and shadow) behavior sigmoidal fits for patients (top, red) and controls (bottom, blue).

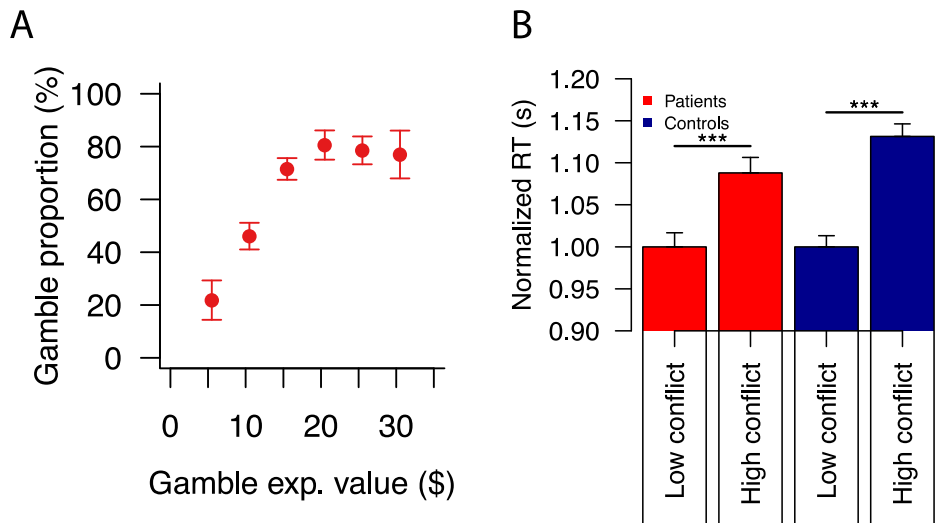

Figure S2: Additional behavioral analyses. Related to Figure 1. (A) average proportion of gambles across patients, depending on the expected value of the gamble. Patients' choices were sensitive to the expected value of the gamble (i.e., the gamble prize times the win probability), with gamble choices more prevalent for higher gamble expected value. (B) Reaction times (RTs) are slowed in trials with harder decisions for both patients and healthy subjects. *Related to Figures 1B and 1C.* We separated trials into high conflict (with win probabilities between 40 and 60%) and low conflict (those with win probabilities either below 30% or above 70%). Patients and healthy subjects took longer to react in high-conflict trials (both $p<0.001$, t-test), and the effect size was comparable between both groups.

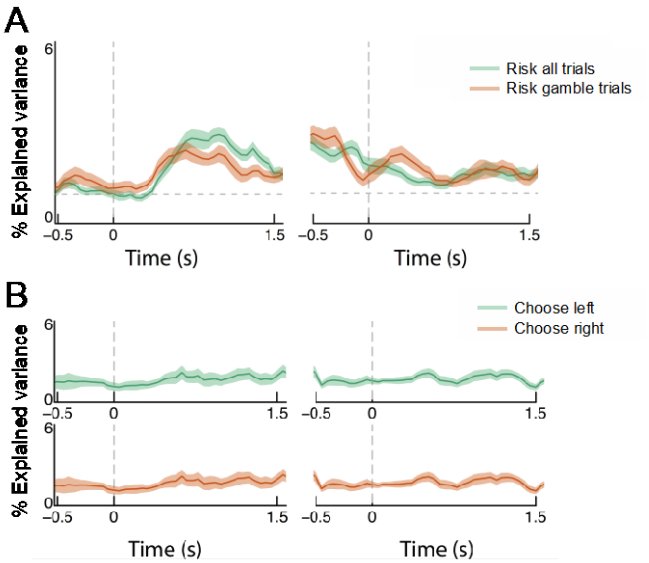

Figure S3: Additional encoding analyses. Related to Figure 3. (A) To verify whether risk information is only relevant when the subject chooses to gamble, we conducted an additional analysis restricting the risk regressor to gamble trials only. We directly compared the %EV of risk encoding in trials in which the patient chose to gamble (orange) vs all trials (green). The regressor including all trials explains a slightly higher proportion of variance in HFA (%EV), suggesting that risk is encoded regardless of subsequent patient choice. (B) Lack of motor encoding in OFC HFA. Regressors encoding direction of choice (left/right options) are not reflected in OFC HFA.

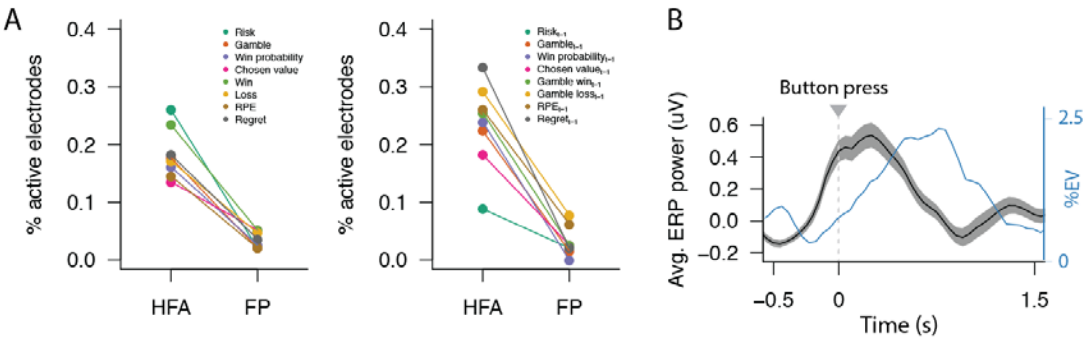

Figure S4: Comparison between HFA and LFP encoding and power modulation. Related to Figures 2-4. (A) HFA captures a significantly greater amount of task-related information than ERPs. Proportion of electrodes encoding each group of reward-related computations across HFA (70-200Hz) and broadband field potentials (FPs). Each joined pair of points represents the proportion of electrodes whose HFA/ERP activity is significantly associated ($p<0.05$) with a given computation; colors indicate different computations. In all instances, the proportion of electrodes encoding information in HFA was significantly greater than in FP (average HFA = 20.9% vs FP = 3.3%, $p<10^{-5}$, t-test). Panels show regressors encoding present (left) and prior round (right) information. (B) Timing of ERP modulation and HFA encoding are different. Average ERP responses across electrodes are shown aligned to patient button press (t=0; black trace, shade indicates SEM). ERP modulation is maximal at the time of button press, and thus does not align in time with maximal encoding of outcome information (win/loss, RPE, regret, shown as blue trace; ~750ms post-outcome reveal) information (Figure 3).

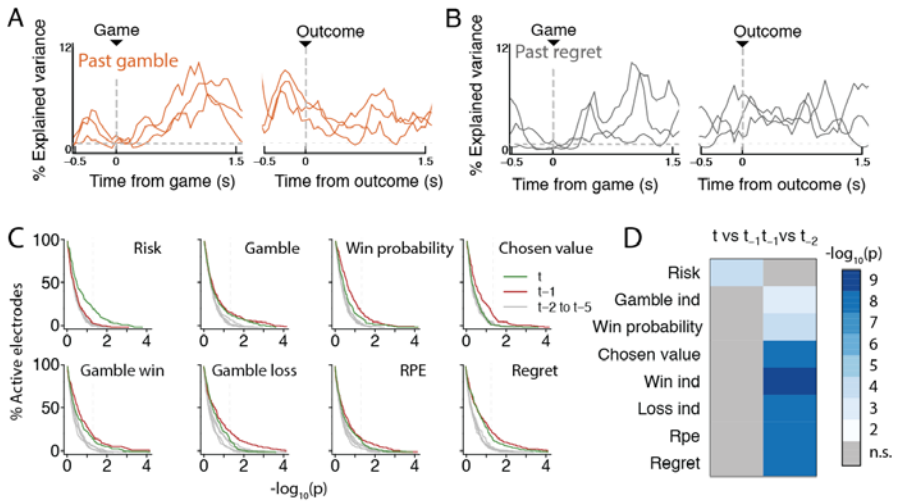

Figure S5: Encoding of past information from the preceding trial. *Related to Figure 4.* (*A*) Three example electrodes encoding past gamble information. Activity is time-locked to the time of initial game presentation (left) and choice/outcome (right) and is expressed as the percentage of variance in the HFA signal accounted for by the risk regression (%EV). (*B*) As (*A*) but for electrodes encoding past regret (parametrized as the extra payoff that would have been obtained by making a different choice in the previous round). Past representation is limited to recent events. *Related to Figure 6.* (*C*) Empirical cumulative distribution functions (ECDFs) of correlation significance ($-\log_{10}(p)$, where p is the p value of the linear regression) across electrodes. Plotted p-values are obtained from the peak %EV time point, which differs across electrodes and past trials (t to t_{-5}). Current trial is indicated in green, previous trial (t-1) in red and earlier trials (t-2 through t-5) in grey. Grey dotted vertical line indicates p=0.05 threshold. (*D*) Summary statistical results for ECDFs in (*C*) highlighting the sharp temporal boundary in encoding extent between t_{-1} and t_{-2}, but not t and t_{-1}. Plot represents the significance ($-\log_{10}(p)$) of comparing the ECDF distributions between t and t_{-1} (left) and t_{-1} and t_{-2} (right; one-sided Kolmogorov-Smirnoff test for $t_{-1}>t$ and $t_{-2}>t_{-1}$, respectively).

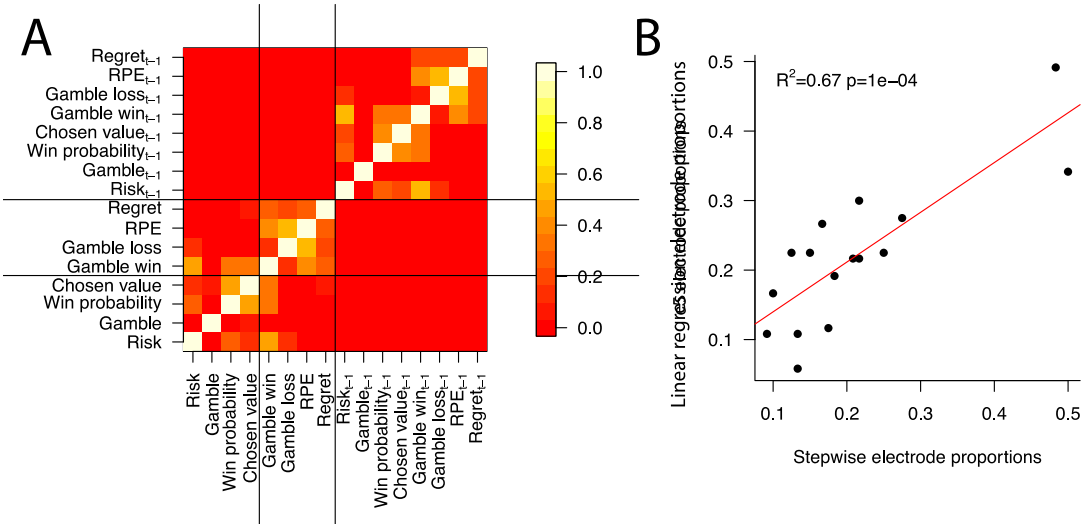

Figure S6: Encoding of multiple reward-related factors is not driven by regressor collinearity. Related to Figures 2-4. (A) Correlation coefficient (R^2) for all pairs of regressors used in the study. Regressors were weakly correlated between and within categories (mean R^2=0.15, all R^2<0.6). (B) Stepwise and individual linear regression show similar results. The proportion of electrodes encoding each reward-related computational component as estimated by selecting electrodes with ≥5 consecutive encoding windows and stepwise regression followed by model selection were similar.

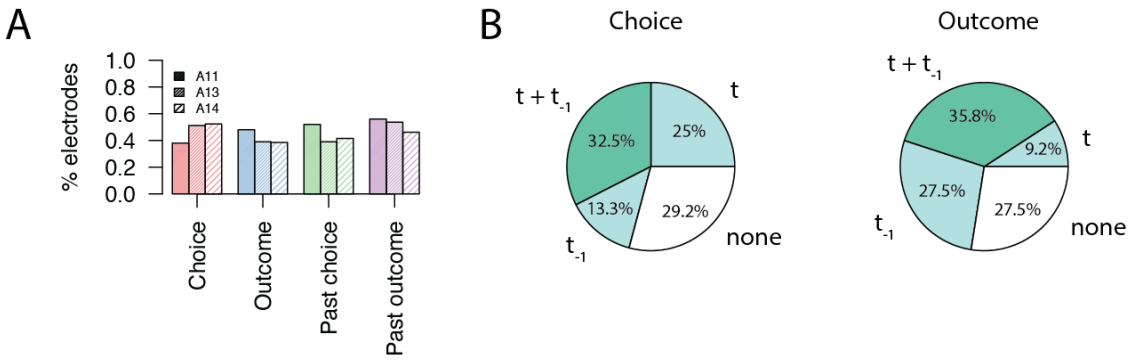

Figure S7: Anatomical location and overlap of different populations of encoding electrodes. Related to Figure 7. (A) Similar proportion of electrodes encode each type of reward-related computational component across OFC subregions. Proportion of electrodes engaged in any type of reward-related computation (choice/outcome/past choice/past outcome) as a proportion of the total number of electrodes in each of the putative Brodmann areas examined (A11, A13, A14). Electrodes encoding present and past outcome overlap. To investigate whether encoding of present and past aspects of the task are encoded by similar groups of electrodes, we compared the distributions of electrodes carrying out present (t), past (t_1), both ($t+t_1$) or no ('none') computations for choice (left) and outcome (right) aspects of the task. We found an overrepresentation of electrodes that encoded both $t+t_{-1}$ regressors both in the case of choice (39/120 or 32.5%, vs. an expected 31/120 or 25.8% under assumption of independence, $p<0.05$, chi-square test) and outcome information (n=43/120, or 35.8% vs. an expected 34/120 or 28.5% under assumption of independence, $p<0.01$, chi-square test).

Table S1. Behavioral regressors. Related to Figure 1.

Regressor	Type/epoch	Formula	Description
Risk	Choice	$\mathbf{E}\{(\mathbf{V}-\mathbf{E}(\mathbf{V}))^2\}$	Risk of gamble option
Gamble index	Choice	$\begin{cases}1 & gamble\\ 0 & safebet\end{cases}$	Boolean – gamble trials
Win probability	Choice	p	Probability of winning
Chosen value	Choice	$\begin{cases}E(p,x)=p\cdot x & gamble\ trials\\ \$10 & safebet\ trials\end{cases}$	Expected value of choice
Win index	Outcome	$\begin{cases}1 & gamble\ win\\ 0 & gamble\ loss/safebet\end{cases}$	Boolean – gamble win trials
Loss index	Outcome	$\begin{cases}0 & gamble\ win/safebet\\ 1 & gamble\ loss\end{cases}$	Boolean – gamble loss trials
Reward prediction error (RPE)	Outcome	$RPE(p,x)=R_t-E(p,x)$	Obtained minus expected reward
Regret	Outcome	$f(p,x)=R_t-max(E_t)$	Obtained minus maximum reward

Notation:

- p = probability of the gamble resulting in a win (e.g. 80% for a shown 2), regardless of patient choice.
- x = potential gamble reward (in $), regardless of patient choice.
- R_t = reward obtained in trial t.
- E(p,x) = expected value of the chosen option, equal to probability times payoff. This is constant for safebet choices (which are certain to result in a $10 prize) and varies round-to-round for gamble choices.
- max(E_t): maximum possible payoff, given the gamble outcome. This is equivalent to $10 in trials in which the gamble resulted/would have resulted in a loss (since the maximum potential payoff was the safebet option), and equal to the gamble payoff in trials which resulted/would have resulted in a win.

Behavioral regressors included in the study. Regressors were initially grouped into choice- and outcome evaluation-related variables, depending on whether they are important prior to action selection (choice) or after the result of the gamble has been revealed (outcome). Regressors were defined on all trials (except timeouts), and could be Boolean (e.g. win index) or parametric (e.g. win probability).

Detailed regressor explanation:

- Risk: measure of uncertainty associated with the presented gamble, regardless of patient choice. Intuitively, risk follows an inverted u-shape, with maximum risk at p=0.5 and minimum at p=0 (sure loss, i.e. a shown 1) and p=1 (sure win, i.e. a shown 0).
- Win probability (p): probability of the gamble resulting in a win (e.g. 80% for a shown 2), regardless of patient choice.

- Chosen value (CV): expected value of the chosen option, defined as the win probability (p) times the potential reward (x, in dollars). CV always equals $10 for safebet choices (p = 1, x = $10) and varies for gamble choices (p = [0,1], x = [10,30]).
- Win/loss index: Boolean indicators for gamble trials that resulted in a win (win index) or a loss (loss index). Always equals 0 for safebet trials.
- Reward prediction error (RPE): deviation from reward expectation, defined as the obtained reward (R_t) minus the expected reward (that is, the chosen value E(p,x)). RPE can take negative (worse than expected), positive (better than expected) or zero (as expected; always the case for safebet trials) values.
- Regret: we operationalized regret as the obtained minus the maximum possible reward, in dollars. Therefore, regret was defined over all trials (whether the subject chose the safebet or the gamble option), and could take values [-20,0]. 0 regret corresponds to ex-post optimal choices (i.e. gamble-win or safebet-loss), whereas negative values correspond to ex-post suboptimal choices (i.e. gamble-loss, which resulted in a fixed regret value of $10, and safebet-win, which resulted in a variable negative regret value equivalent to the gamble prize minus the $10 dollars gained from the safebet).

Table S2. Number of electrodes encoding individual reward-related computations across patients. Related to Figures 1-4.

Regressor	**s01**	**s02**	**s03**	**S04**	**s05**	**s06**	**s07**	**s08**	**s09**	**s10**
Risk	1	1	25	0	14	0	0	3	4	2
Gamble	2	1	7	0	14	0	1	4	3	2
Offer value	0	0	6	1	9	0	1	6	7	1
Chosen value	0	0	5	2	8	0	3	1	6	1
Any choice encoding[1]	2	1	30	1	36	4	6	5	8	8
Win index	0	1	7	0	16	0	0	5	13	3
Loss index	3	1	2	0	14	0	3	1	8	1
RPE	0	1	2	0	10	0	2	1	11	1
Regret	0	3	4	1	14	0	1	2	6	4
Any outcome encoding[1]	3	3	12	1	29	0	4	8	17	5
Past risk	0	0	4	0	4	0	1	2	6	0
Past gamble	1	2	9	1	12	0	2	6	4	6
Past win probability	0	2	6	1	18	4	2	5	5	3
Past chosen value	0	1	8	1	14	4	2	3	2	0
Any past choice[1]	1	2	19	1	28	6	2	6	15	7
Past win index	0	2	9	1	22	1	1	5	6	2
Past loss index	1	0	1	2	35	1	6	0	7	3
Past RPE	0	1	8	1	21	1	4	1	11	2
Past regret	3	1	14	3	36	0	2	2	1	2
Any past outcome[1]	4	3	18	4	44	2	7	5	11	6
Total task active electrodes	5	4	44	5	54	7	10	9	17	12
Total # electrodes	5	6	52	5	61	7	11	10	19	16

[1] Number of unique electrodes associated with reward-related computations.